Renewable Energy 101 (2017) 90–95

Contents lists available at ScienceDirect

Renewable Energy

journal homepage: www.elsevier.com/locate/renene

Front contact optimization of industrial scale CIGS solar cells for low solar concentration using 2D physical modeling

Jose-Maria Delgado-Sanchez [a, *], Juan M. López-González [b], Albert Orpella [b], Emilio Sánchez-Cortezon [b], María D. Alba [c], Carmen López-López [a], Ramón Alcubilla [b]

[a] Abengoa, C/ Energia Solar 1, 41014, Sevilla, Spain
[b] Micro and Nano Technologies Group, Departament d'Enginyeria Electrònica, Universitat Politècnica de Catalunya, C/ Jordi Girona 1-3, Mòdul C4, 08034, Barcelona, Spain
[c] Instituto Ciencia Materiales de Sevilla – (CSIC-US), Avda. Americo Vespuccio 49, 41092, Sevilla, Spain

ARTICLE INFO

Article history:
Received 21 April 2016
Received in revised form
25 July 2016
Accepted 22 August 2016

Keywords:
Concentrating solar power
Concentrator
Thin-film
Solar energy
Photovoltaic cells
Semiconductor device modeling

ABSTRACT

$Cu(In,Ga)Se_2$ (CIGS) technology is one of the best absorber materials with record efficiencies among photovoltaic thin-film technologies (22.3% at lab scale and 16% at large commercial module). Although research on this material was originally motivated by low-cost, glass-glass applications focusing to fixed photovoltaic structures, the high efficiency values make CIGS an interesting alternative for low concentration systems. In this paper a 2D model for $Cu(In,Ga)Se_2$ (CIGS) solar cells under low solar concentration is described and contrasted with experimental data. Using simulation, the effect of front electric contact design parameters: finger width, finger separation, and number of buses are analyzed for solar concentrations from 1 up to 10 suns. Efficiency maps allowing front contact grid optimization are shown and analyzed for each concentration factor (Cx), assessing the viability of CIGS solar cells for low concentration applications, where commercial CIGS solar cells may exhibit 35% of electrical power increases with proper front grid optimization under low concentration respect to conventional grid design.

1. Introduction

Nowadays CuIn1-xGaxSe$_2$ (CIGS) is one of the most efficient thin film technologies attracting great interest from the scientific and industrial photovoltaic community [1–3]. Efficiencies exceeding 22% have been obtained at the laboratory scale [4] and the technology has reached an industrial maturity with efficiencies over 16% at the module level [5]. Nevertheless the scarcity of In and Ga may limit the success of this technology and new alternatives are being actively researched [6]. Among them, kesterites are candidates of choice although the technological complexities raise doubts about its industrial feasibility.

Optical concentration may be an interesting alternative for CIGS technology because it allows the reduction of cell area whereas the output power is maintained and consequently the use of rare and expensive materials could be minimized. Very little work has been done in concentration applications of CIGS solar cells. Some studies about small surface CIGS solar cells under high concentration have been performed [7–9], however in this range of dimensions ($<10^{-1}$ cm^2 and 10^{-6} cm^2) grid effects and, in general, series resistance is negligible due to the small dimensions of the cells. When solar cell is operating under concentration level for larger cell areas, series resistance contribution from front grid is a critical issue because photogenerated current density increases and electrode conventional design becomes increasingly important in order to avoid ohmic losses. This field is still largely unexplored due to this limiting effect of series resistance in thin film solar cells.

The aim of this work is the optimization of the front grid design through the exploration of the large surface CIGS solar cells in low solar concentration (LCPV) installations. 2D device simulator (ATLAS from SILVACO [10]) has been used. Firstly, and for tuning the model, the simulation results are validated for a large area CIGS based solar cell. Secondly, the capabilities of those cells under low solar concentration (up to 10 suns) have been explored to optimize the front contact grid design (finger width, separation between fingers and number of buses) for each solar concentration factor.

* Corresponding author.
E-mail address: josemaria.delgado@abengoa.com (J.-M. Delgado-Sanchez).

http://dx.doi.org/10.1016/j.renene.2016.08.046
0960-1481/

2. Material and methods

The scope of this work is described in this section. An accurate simulation framework needs to consider the proper parameters of the materials involved in the device. Different characterization techniques have been used for this investigation and the results are used when simulating the CIGS solar cell. Finally, simulations results are validated at different concentration levels through comparison with measured ones (section 3).

2.1. Experimental characterization

A reference solar cell based on CIGS thin-film technology was used. Cross section and geometry parameters are shown in Fig. 1 and Fig. 2, respectively. Silver fingers are 385 μm width separated 2330 μm. Active solar cell layers thicknesses are respectively: In_2O_3:SnO_2 (ITO) 150 nm, Al:ZnO 200 nm, ZnO 50 nm, CdS 50 nm and CIGS 1500 nm.

Material properties, in particular real Ga composition in the absorbing layer, are fundamental to establish accurate physical model of CIGS solar cell, for this reason XRD and Raman Spectroscopy experimental methods used are explained in detail.

XRD measurements using a PANalytical X'Pert PRO MPD (model DY 3197) difractometer were performed on the absorber samples (after etching of ITO and buffer layers using one HCl 10% wt solution for 5 min). The analysis was made between 10° up to 75° 2θ.

In-depth resolved Raman-AES (Auger Electron Spectroscopy) measurements on the absorber were carried out aiming to identify the chemical phases, using T64000 Horiba Jobin-Yvon spectrometer. Excitation was provided through the 514.5 nm emission line of an Ar^+ laser and measurements were performed in backscattering configuration. Combined in-depth Raman/AES measurements were made by sequentially acquiring a series of Raman spectra after sputtering the sample with the Ar^+ beam from Phi 670 scanning Auger nanoprobe. To minimize damage in the sputtered region, the energy of the Ar^+ beam during ion sputtering was below 5 keV.

Performance (I-V curve) of solar cells under different illumination levels were characterized using an in-house solar simulator AAA class with spectral and temperature control. It is based on multi-flash illumination system, able to reach concentration 1000 suns with the required light collimation by means of a large-area parabolic mirror, which collimates the divergent light beam coming from a small Xenon flash bulb.

2.2. Model description

1D CIGS solar cells simulations have been previously reported [10]. However, in a pure 1D model, some aspects of the solar cell, in particular those related with the collection of carriers at the front grid, cannot be analyzed. In this work, we use a 2D simulator [11] which allows the analysis of the device performance when the front grid design is modified, obtaining optoelectronic devices performance. Materials and device structure varies in the vertical direction while the variation in the horizontal direction is going to be defined by the finger/bus geometry and distribution.

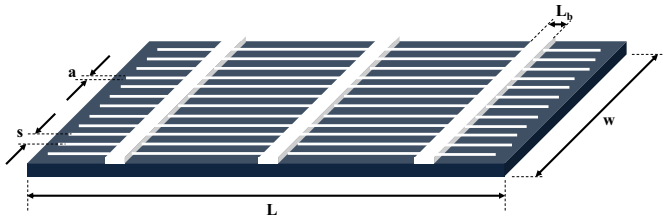

Fig. 1. Conventional front-grid design for CIGS solar cells.

Table 1 shows the parameters used for the different materials within the cell required for the modeling: doping concentration (ND/NA), relative dielectric constant (ε), gap (Eg), electronic affinity (χ), effective density of states both in conduction and valence bands (N_c and N_v), recombination lifetimes ($\tau_{n,eff}$ and $\tau_{p,eff}$), carrier mobilities (μ_n and μ_p) and defect donor or acceptor like characteristics (a mid-gap gaussian defect continuous model is used) [12], total density of states (N_{GD} or N_{GA}), peak energy (E_{GD} or E_{GA}), characteristic decay energy (ω_{GD} or ω_{GA}), electron capture cross-section (σ_{eGD} or σ_{eGA}), and hole capture cross-section (σ_{hGD} or σ_{hGA}). All these parameters are considered as input data to SILVACO software simulation.

Some of the parameters of Table 1 were extracted from the literature [13,14]. Other parameters like Ga composition in the absorbing layer has been measured through XRD and Raman/AES measurements. Ga content showed a gradient along the absorber layer, approximately between 0.33 and 0.67 while the corresponding gap varies between 1.24 and 1.46 eV. This value has deep consequences in the quantum efficiencies for the high wavelength region of the solar spectrum and consequently in the short circuit current. Additionally, the average value of the CIGS layer gap affects also the dark saturation current density and the open circuit voltage [15,16]. The gap values within the CIGS layer and its dependence with Ga composition is a controversial question because some discrepancy exists between experimental and theoretical values [17–21].

Complex refraction index for the semiconductor regions (ZnO, CdS, CIGS) used in the simulation of the optical behavior of the solar cell has spectral dependence [22]. In addition ITO layer is modeled with refraction real index equal to 2. ITO is considered in the simulation as a highly doped semiconductor with a 3.7 eV gap [23,24] with a resistivity of 1000 μΩ cm (sheet resistance of 67 Ω/sq), and a contact resistance with the metallic Ag fingers of 0.13 Ω cm^2. Additionally, a surface recombination velocity at the interface CdS/CIGS of $3 \cdot 10^4$ cm s^{-1} has been taken into account. Since this work is mostly concerned with front grid optimization, the back contact has been substituted by a single metallic contact reproducing an effective contact resistance of 1.0 Ω cm^2. The bidimensional structure in Fig. 1 is completed with an external resistance taking into account the experimentally measured resistivity of the fingers (40 μΩ cm) and the resistance introduced by the buses (60 μΩ).

3. Results

3.1. Solar cell microstructure

To obtain accurate simulation results it is necessary to have detailed knowledge about microstructure, composition, optical and electronic properties of involved materials. In particular, the Ga content is critical for the photovoltaic performance of the CIGS solar cell and needs to be known for a proper simulation. In order to assess this value, XRD and in-depth resolved Raman Spectroscopy were performed.

Fig. 3 corresponds to a detailed image of the (112) CIGS XRD reflection measured on the CIGS solar cell used in this work. This spectrum has a complex shape, resulting from the contribution of regions with different Ga content and it can be fitted by means of three contributions corresponding to CIGS with Ga/(In + Ga) fraction between 43% and 76%. These compositions approximately agree with the range of values obtained from the in-depth resolved Raman measurements, as will be described later. Estimation of the relative Ga content is based on the assumption of the validity of

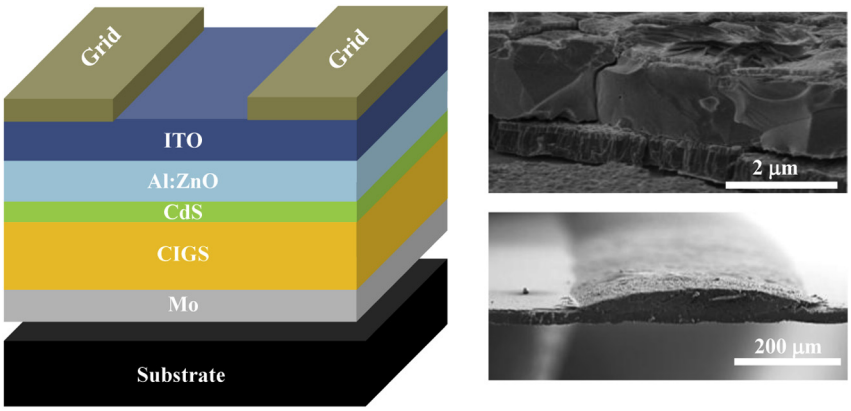

Fig. 2. Left, geometry and materials used for the solar cell modeling; right, SEM images of the solar cell used on the experimental characterization.

Table 1
Semiconductor Properties used in the modeling.

Parameter	Units	ITO	ZnO:Al	CdS	CIGS
N_D/N_A	cm^{-3}	6.25×10^{19}	1.00×10^{18}	1.00×10^{17}	1.00×10^{16}
ε	–	9	9	10	13.6
E_g	eV	3.7	3.3	2.4	1.2–1.5
χ	eV	4.6	4.6	4.4	4.5
N_c	cm^{-3}	2.2×10^{18}	2.2×10^{18}	2.2×10^{18}	2.2×10^{18}
N_v	cm^{-3}	1.8×10^{19}	1.8×10^{19}	1.8×10^{19}	1.8×10^{19}
$\tau_{n,eff}$	S	1×10^{-7}	1×10^{-7}	1×10^{-7}	1×10^{-7}
$\tau_{p,eff}$	S	1×10^{-7}	1×10^{-7}	1×10^{-7}	1×10^{-7}
μ_n	$(cm^2)/(V \cdot s)$	100	100	100	50
μ_p	$(cm^2)/(V \cdot s)$	25	25	25	20
Def. type	–	donor	donor	acceptor	donor
N_{GD}/N_{GA}	cm^{-3}	1×10^{17}	1×10^{17}	1×10^{18}	1×10^{14}
E_{GD}/E_{GA}	eV	1.85	1.65	1.20	0.58
w_{GD}/w_{GA}	eV	0.1	0.1	0.1	0.1
$\sigma_{eGD}/\sigma_{eGA}$	cm^2	1×10^{-12}	1×10^{-12}	1×10^{-17}	5×10^{-13}
$\sigma_{hGD}/\sigma_{hGA}$	cm^2	1×10^{-15}	1×10^{-15}	1×10^{-12}	1×10^{-15}

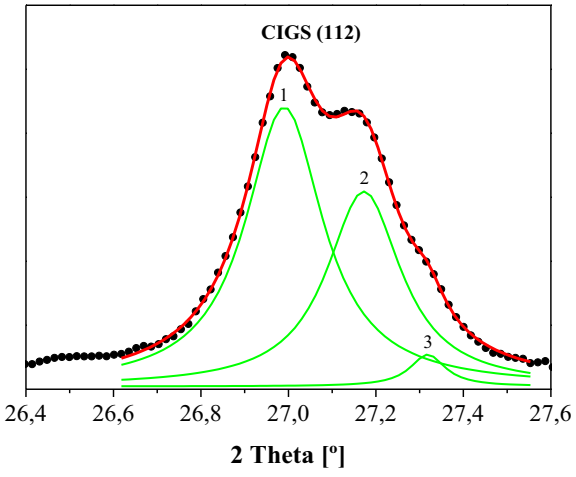

Fig. 3. Detail of the XRD pattern of the solar cell used, showing the fitting of the CIGS (112) reflection with three contributions related to the response of absorber regions with different Ga/(In + Ga) relative content (43% reflection 1, 61% reflection 2 and 76% reflection 3 respectively).

Vegard's law, which predicts a linear dependence of the average lattice constant in the alloy with the relative Ga content. Then, in the modeling of the solar cell a gradual increase in the Ga/(In + Ga) fraction content with thickness in the absorber will be used, from values about 33% at the surface up to a value of the order of 67%.

For Raman characterization (Fig. 4), surface is etched with ion bombarding, to get information from the surface to CIGS/Mo interface. These spectra are characterized by a dominant peak corresponding to the vibrational ground state A1 mode from the CIGS phase. The main feature in these spectra is the existence of a gradual blue shift of the A1 CIGS mode that increases with depth in the absorber. This blue shift is not accompanied by a corresponding increase of the Full Width at Half Maximum (FWHM) of the mode. This allows ruling out a structural disorder related with the blue shift of the mode. Then, the shift has been attributed to a gradual increase in the relative Ga/(In + Ga) content with the depth in the absorber, from values in the surface region about 33% up to a value around 67%. This agrees [25] with the Ga/(In + Ga) relative content values estimated at these regions from the XRD diffractogram.

3.2. Model validation

First step of the simulation consists to validate the model. It means that data obtained from the modeling will be compared with experimental results. For this purpose, one CIGS solar cell, which is described on previous section, has been characterized (I-V curve at different radiations level) using a solar simulator at different levels of radiation concentration. Fig. 5 show the simulated and experimental results under different levels of sun concentration, demonstrating good fitting between predicted and experimental values.

A good agreement between experimental and simulated data was observed. On the other hand a drastic reduction in efficiency was predicted and experimentally observed when going from 1 to 10 suns. This is consequence of high serial resistance in the device due to the intrinsic properties of the semiconductor. The effect of this series resistance increases when solar cell is exposed to higher levels of radiation. In order to overtake this drawback of CIGS absorber the design of the front-grid has to be optimized to ensure proper extraction of generated photocarriers. This result demonstrates that a careful design of the front metallic grid is mandatory for concentrated sunlight applications; otherwise, the capabilities of the device will be severely degraded.

3.3. Front contact optimization

Once the solar cell simulation framework is properly validated and its predictions compared with experimental results, it will be used to optimize the front-grid design for low concentration conditions. This section presents the effect on the solar cell efficiency of the following design parameters of the front electric contact: Finger

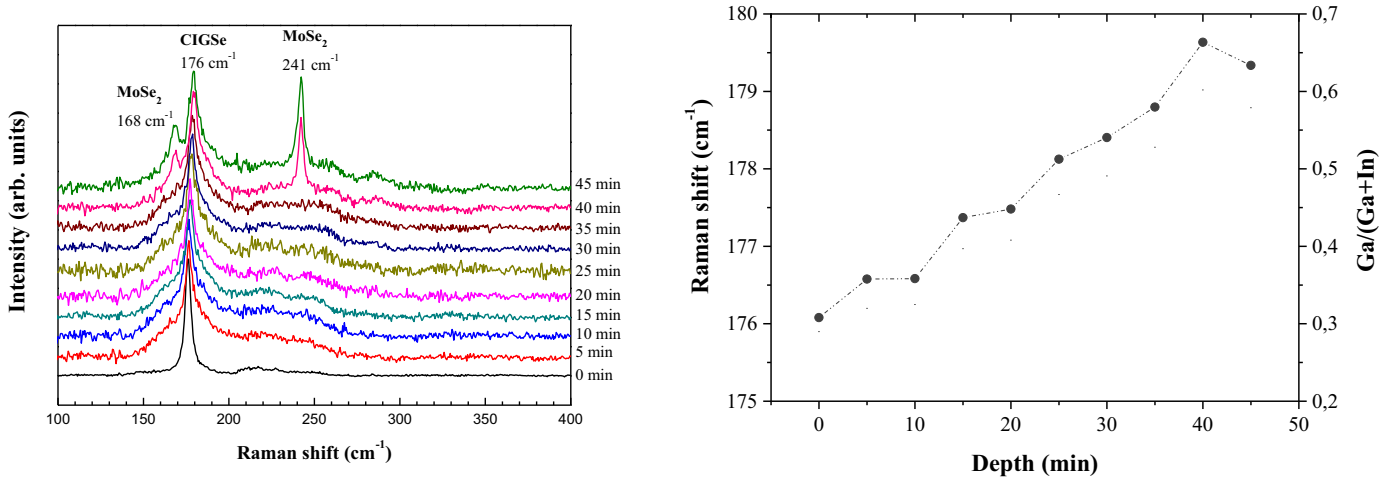

Fig. 4. Raman spectra taken at different sputtering times (left) and detail of Raman Shift of the A1 CIGSe mode according Ga distribution in the absorber layer.

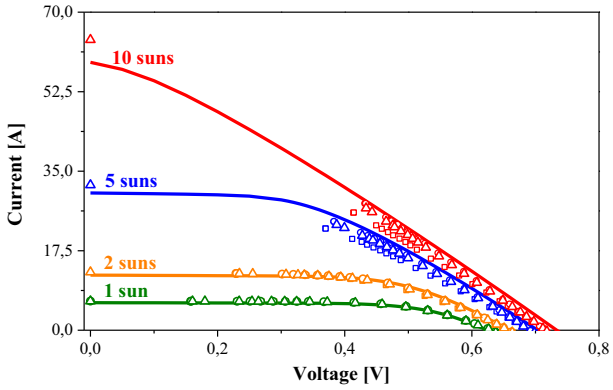

Fig. 5. I-V lighted results of simulated reference CIGS solar cell (lines) compared with measured of three random CIGS experimental solar cells (A – square marks-, B –circle marks-, and C –triangle marks-), under four different levels of sun concentration (1×, 2×, 5×, and 10×).

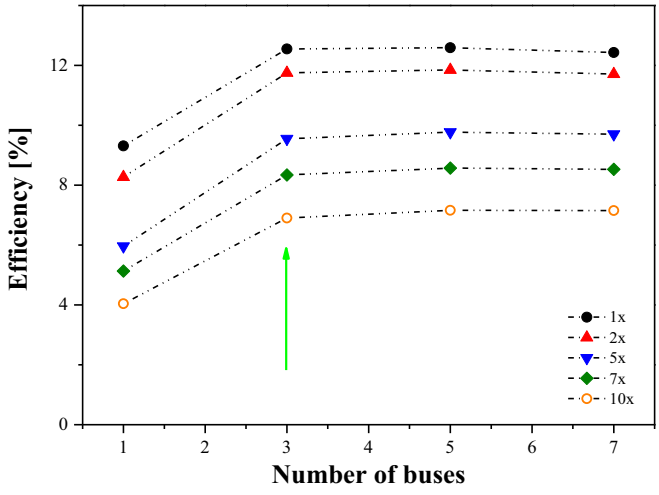

Fig. 6. Influence on the efficiency due to number of buses employed on the front-grid, simulated at different radiation concentration factors.

width a, finger separation s, number of buses n_b, for 1×, 2×, 5×, 7× and 10× sun concentrations. The rest of geometrical parameters were fixed, W = 10 cm, L = 21 cm, L_b = 0.2 cm, as they were described at Fig. 1.

The current generated by the solar cell is collected through the buses, so it is needed to take into account the effect of thermal losses that can provoke a detrimental performance of the cell. Basing on that, the first factor to consider on the modeling is the number of buses used to collect the current in order to try to minimize performance losses in the device, due to Joule effect and moreover to optimize the cost design.

The performance of the device under concentration improves when the number of buses employed increases from 1 to 3. However there is a clear plateau between 3 and 7 buses for all values of concentration. Although the optimum value seems to be 5 buses (Fig. 6), in order to compensate optimum value with cost optimization, the number of buses proposed as optimum design was fixed to 3.

Secondly, once the number of buses has been fixed to 3 ($n_b = 3$) we optimized both finger width and finger separation for different values of the concentration factor incident on the solar cell, in order to ensure that any carrier generated on the semiconductor is properly transported to the nearest bus avoiding excessive ohmic losses; as it can be observed in Fig. 7, best recommendation is to use maximum number of fingers as possible, but narrowest width to minimize shadow losses.

Fig. 7 shows the simulated efficiency maps for ×1 sun (Fig. 7a), ×2 suns (Fig. 7b), ×5 suns (Fig. 7c) and ×10 suns (Fig. 7d) obtained as a function of finger width and separation, please note that figures for ×1 or ×2 suns and for ×1 or ×10 suns have different vertical axis scales in order to show clearly the different regions. This theoretical analysis allows us to obtain the optimized front-grid design to achieve the CIGS highest efficiency depending on the concentration factor. Such results are summarized in Table 2.

On the other hand, these results also reveal that a significant performance enhancement on the CIGS solar cell can be achieved considering rather broad conditions for finger specifications. For example: at ×5 suns, a good efficiency (10.4%), near the optimum value (10.5%), is achieved, for example, with s = 1500 μm and a = 370 μm; and for ×10 suns, a good efficiency (8.3%), near the optimum value (8.4%), is achieved with s = 1000 μm and a = 370 μm.

Finally, the optimized grid design is compared with the experimental data (I-V curve presented in previous section) from the reference CIGS cell (s = 2330 μm and a = 385 μm). As it can be seen in Fig. 7, when no concentration or minor concentration factor is

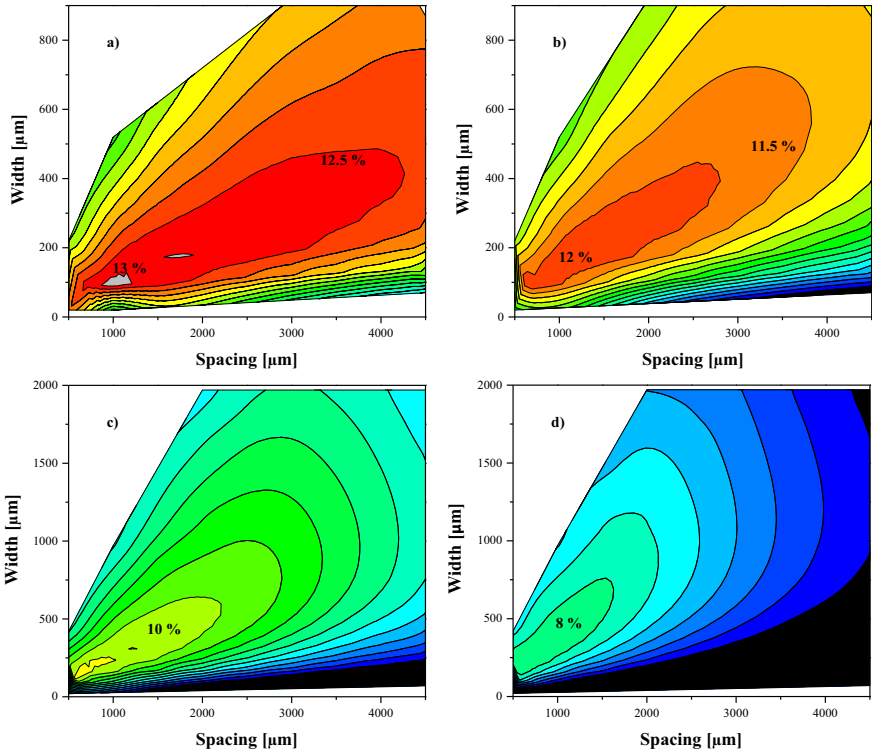

Fig. 7. Efficiency maps versus finger width a, and finger spacing s for: a) 1 sun, b) 2 suns, c) 5 suns, and d) 10 suns concentrations.

Table 2
Efficiency for different Concentration Factors, as function of metallic grid design.

Cx factor	Efficiency with optimized solar cell	Finger width [µm]	Finger distance [µm]
1x	13.0	120	1500
2x	12.4	70	500
5x	10.5	120	500
10x	8.4	170	500

considered there are no relevant differences between optimized front-grid solar cell and conventional device. However it should be noted that when concentration factor is higher than 5x, a correct front grid design is crucial to achieve a high performance of the solar cell.

Based on the results presented, conventional electrical front-grid must be redesigned for low concentration radiation operation conditions. Otherwise, front grid will not be able to extract charge carriers efficiently due to the high series resistance of the solar cell and solar cell performance will be under expectation. This work has demonstrated how electrical power produced by the solar cell can be enhanced (Fig. 8) when front-grid is optimized according the incoming illumination level.

4. Conclusions

A physical 2D model for CIGS thin film solar cells has been developed. Information about the microstructure and composition was obtained by XRD and Raman Spectroscopy; in this way the dependence of absorber band gap with Ga content can be properly considered. The model developed is able to predict the solar cell performance under different concentration factors.

Results demonstrate that by using optimized front contact grid, CIGS thin-film solar cells may improve their r performance under low concentration conditions: when concentration factor used is

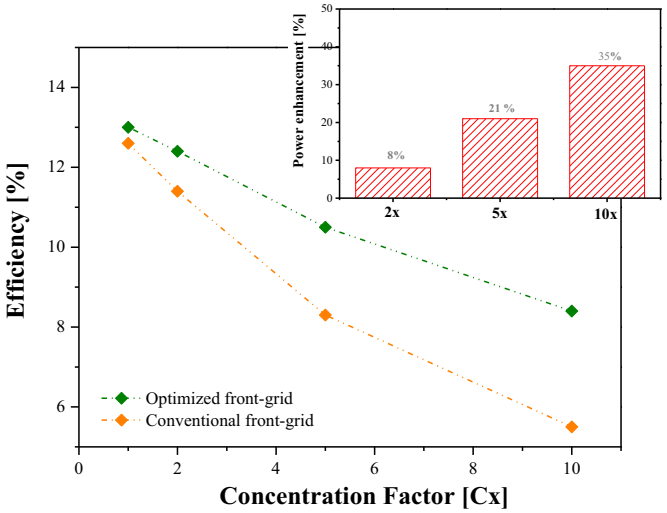

Fig. 8. Efficiency and electrical power enhancement comparison with a conventional electrical front-grid obtained from I-V curve at STC 1x, and optimized design for CIGS solar cell under low concentration radiation (2x, 5x and 10x).

10x, efficiency goes from 5.5% to 8.4%, which also means a 35% in electrical power generation. Although reference commercial solar cell matched the optimum performance at 1x sun, narrowing the finger spacing and fine tuning the finger size allow substantial gain of efficiency at higher concentration factors.

These results, using reference industrial scale CIGS solar cells open interesting perspectives for thin film solar cell use under concentrated sunlight. Cost per watt may be reduced because under concentration smaller area cells can be used and smaller amounts of precursor materials are needed.

It has been also demonstrated that the polycristalline structure of the CIGS technology and their inherent defects do not represent one limitation to explore concentration concepts.

References

[1] M. Powalla, P. Jackson, W. Witte, D. Hariskos, S. Paetel, C. Tschamber, W. Wischmann, High-efficiency Cu(In,Ga)Se2 cells and modules, Sol. Energy Mater. Sol. Cells 119 (2013) 51–58.

[2] A. Jager-Waldau, Progress in chalcopyrite compound semiconductor research for photovoltaic applications and transfer of results into actual solar cell production, Sol. Energy Mater. Sol. Cells 95 (2011) 1509–1517.

[3] S. Niki, M. Contreras, I. Repins, M. Powalla, K. Kushiya, S. Ishizuka, S. Matsubura, CIGS absorbers and processes, Prog. Photovol. Res. Appl. 18 (2010) 453–466.

[4] http://www.solar-frontier.eu/(News published 08-12-2015).

[5] http://www.manz.com/markets/solar/cigs-fab/.

[6] T.K. Todorov, J. Tang, S. Bag, O. Gunawan, T. Gokmen, Y. Zhu, D.B. Mitzi, Beyond 11% efficiency: characteristics of state-of-the-art Cu2ZnSn(S,Se)4 solar cells, Adv. Energy Mater. 3 (2013) 34–38.

[7] M. Paire, L. Lombez, N. Pere-Laperne, S. Collin, J.L. Pelouard, D. Lincot, J.F. Guillemoles, Microscale solar cells for high concentration on polycrystalline Cu(In,Ga)Se_2 thin films, Appl. Phys. Lett. 98 (2011) 264102.

[8] M. Paire, L. Lombez, F. Donsanti, M. Jubault, S. Collin, J.J. Pelouard, J.F. Guillemoles, D. Lincot, Cu(In,Ga)Se2 microcells: high efficiency and low material consumption, J. Renew. Sustain. Energy 5 (2013) 011202.

[9] J.S. Ward, K. Ramanathan, F.S. Hasoon, T.J. Coutts, J. Keane, M.A. Contreras, T. Moriarty, R. Noufi, A 21.5% efficient Cu(In,Ga)Se2 thin-film concentrator solar cell, Prog. Photovol. Res. Appl. 10 (2002) 41–46.

[10] Silvaco 2015 http://www.silvaco.com.

[11] Silvaco, Atlas User's Manual Subsection 14.2 – Simulating TFT Devices, 2013, pp. 738–739.

[12] C.H. Huang, Effects of Ga content on Cu(In,Ga)Se2 solar cells studied by numerical modeling, J. Phys. Chem. Solids 69 (2008) 330–334.

[13] N. Khoshsirat, N.A. Yunus, M.N. Hamidon, S. Shafie, N. Amin, Analysis of absorber layer properties effect on CIGS solar cell performance using SCAPS, Optik 126 (2015) 681–686.

[14] B.M. Hack, J.G. Shaw, Numerical simulations of amorphous and polycrystalline silicon thin-film transistors, in: 22nd International Conference on Solid-state Devices and Materials, 1990, pp. 999–1002.

[15] P. Chelvanathan, M.I. Hossain, N. Amin, Performance analysis of copper-indium-gallium-diselenide (CIGS) solar cells with various buffer layers by SCAPS, Appl. Phys. 10 (2010) 387–391.

[16] M. Gloeckler, J.R. Sites, Efficiency limitations for wide-band-gap chalcopyrite solar cells, Thin Solid Films 480–481 (2005) 241–245.

[17] I. Repins, M.A. Contreras, B. Egaas, C. Dehart, J. Scharf, C.L. Perkins, B. To, R. Naufi, 19.9% efficient ZnO/CdS/CuInGaSe2 solar cell with 81.2% fill factor, Prog. Photovol. Res. Appl. 16 (2008) 235–239.

[18] K. Decock, S. Khelifi, M. Burgelman, Analytical versus numerical analysis of back grading in CIGS solar cells, Sol. Energy Mater. Sol. Cells 95 (2011) 1550–1554.

[19] B. Vermang, V. Fjällstrom, J. Pettersson, P. Salome, M. Edoff, Development of rear surface passivated Cu(In,Ga)Se2 thin film solar cells with nano-sized local rear point contacts, Sol. Energy Mater. Sol. Cells 117 (2013) 505–511.

[20] I.L. Repins, B.J. Stanbery, D.L. Young, S.S. Li, W.K. Metzger, C.L. Perkins, W.N. Shafarman, M.E. Beck, L. Chen, V.K. Kapur, D. Tarrant, M.D. Gonzalez, D.G. Jensen, T.J. Anderson, X. Wang, L.L. Kerr, B. Keyes, S. Asher, A. Delahoy, B.V. Von Roedern, Comparison of device performance and measured transport parameters in widely-varying Cu(In,Ga)(Se,S), Prog. Photovol. Res. Appl. 14 (2006) 25–43.

[21] H.-H. Sung, D.-C. Tsai, Z.-C. Chang, B.-H. Kuo, Y.-C. Lin, T.-J. Lin, S.-C. Liang, F.-S. Shieu, Ga gradient behavior of CIGS thin film prepared through selenization of CuGa/In stacked elemental layers, Surf. Coatings Technol. 259 (2014) 335–339.

[22] M. Gilic, J. Trajic, N. Romcevic, M. Romcevic, D.V. Timotijevic, G. Stanisic, I.S. Yahia, Optical properties of CdS thin films, Opt. Mater. 35 (2013) 1112–1117.

[23] M. Gloeckler, Device Physics of Cu(In,Ga)Se2 Thin-film Solar Cells, Ph.D. Thesis in Colorado State University, 2005.

[24] K. Fleischer, E. Arca, I.V. Shvets, Improving solar cell efficiency with optical optimized TCO layers, Sol. Energy Mater. Sol. Cells 101 (2012) 262–269.

[25] X. Fontane, V. Izquierdo-Roca, L. Calvo-Barrio, A. Perez-Rodriguez, J.R. Morantes, D. Guettler, A. Eicke, A.N. Tiwari, Investigation of compositional inhomogeneities in complex polycrystalline Cu(In,Ga)Se2 layers for solar cells, Appl. Phys. Lett. 95 (2009) 261912.